Hydraulic modelling of bridges in two-dimensional shallow water models

Luis Cea[1], Gabriela Vila[2], Gonzalo García-Alén[3], Jerónimo Puertas[4] and Luis Pena[5]

[1]Professor, Water and Environmental Engineering Group, Department of Civil Engineering, Universidade da Coruña, 15071 A Coruña, Spain. Email: luis.cea@udc.es

[2]Assistant Researcher, Water and Environmental Engineering Group, Department of Civil Engineering, Universidade da Coruña, 15071 A Coruña, Spain. Email: gabriela.vila.sanchez@udc.es

[3]Ph.D. Candidate, Water and Environmental Engineering Group, Department of Civil Engineering, Universidade da Coruña, 15071 A Coruña, Spain. Email: g.glores@udc.es

[4]Professor, Water and Environmental Engineering Group, Department of Civil Engineering, Universidade da Coruña, 15071 A Coruña, Spain. Email: jeronimo.puertas@udc.es

[5]Professor, Water and Environmental Engineering Group, Department of Civil Engineering, Universidade da Coruña, 15071 A Coruña, Spain. Email: luis.pena@udc.es

Corresponding author: Luis Cea (luis.cea@udc.es)

Abstract

The backwater effect generated by bridges can significantly contribute to increase the risk of flooding. In this work we compare two different methods to include the effect of bridges in 2D shallow water models. The first method is based on empirical discharge equations that are implemented as internal conditions. The second method is the recently proposed 2D extension of the Two-component Pressure Approach, which accounts for the vertical confinement of the flow. Both approaches are tested and compared using a new set of experimental data obtained in 32 laboratory tests, including 4 different bridge geometries under different flow conditions. The results show that both methods can reproduce the observed bridge afflux for a wide range of flow conditions, but the Two-component Pressure Approach is less dependent on model calibration. On the other hand, both methods fail to correctly reproduce the 2D water depth patterns observed around the bridge.

This version of the article has been accepted for publication, after peer review, but is not the Version of Record and does not reflect post-acceptance improvements, or any corrections. The Version of Record is available online at: https://doi.org/10.1061/(ASCE)HY.1943-7900.0001992

Introduction

The evaluation of river inundation risk relies largely on the performance of two-dimensional shallow water models (Areu et al. 2019; Bermúdez et al. 2019; Costabile and Macchione, 2015; Fraga et al. 2020; Garrote et al. 2016; Ocio et al. 2016). The accuracy and computational efficiency of these models, as well as the availability of the required input data, have increased over the last years and currently, they are able to provide reliable flood hazard estimations over entire river floodplains and urban areas. However, the acccuracy of two-dimensional shallow water models might deteriorate in the presence of inline structures as bridges, culverts or weirs. In the surroundings of these structures, the hydrostatic pressure approximation, which is an essential assumption in the shallow water equations, is no longer valid. Moreover, in the presence of bridges and culverts, the movement of the water surface might be constrained by the bridge deck or by the culvert crown, generating complex mixed free-surface-pressurised flow conditions. Even if the shallow water approximations are only broken locally, the fact of modelling inaccurately the flow field will have an effect on the head loss generated by the hydraulic structure, which in turn will affect the flood extension in the whole upstream river reach. Especially when the terrain is relatively flat, this can result in several hundred meters of error in the horizontal extension of the flood.

The backwater effect of bridges has been experimentally investigated in several previous studies. The most thorough experimental research on bridge hydraulics was carried out by the U.S. Army Corps of Engineers (USACE) and the Federal Highway Administration (FHA) since the 1950's (Hunt, 1995; Shearman et al., 1986). Their pioneer works contributed to the development of well-established empirical equations and methods for the computation of head losses at bridges that are still used today in many 1D river hydraulics models as HEC-RAS (Brunner, 2010; Shearman et al. 1986). Hamill (1999) provides several simple equations that can be manually applied to estimate the hydraulic effect of bridges. Since these formulations are intended to be used in 1D computations of backwater curves, they must account not only for the flow resistance generated by the deck and the piers, but also for the head losses produced by the contraction and expansion of the flow upstream and downstream from the bridge cross section. In fact, several studies, as those by Hunt (1995) and by Hunt et al. (1999) for the U.S. Army Corps of Engineers, are focused on the accurate evaluation of the

contraction and expansion losses in 1D models, which implies the definition by the user of up to 6 intermediate cross-sections, as well as several contraction and expansion ratios and coefficients and the relative roughness of the floodplains and main stream. Later on, Seckin et al. (2007) recognised the difficulty for the user to define all these case-dependent coefficients, which can lead to considerable inaccuracies in practical applications, and proposed a simplified method to evaluate energy losses under free-surface conditions (i.e. non-submerged bridges). On the other hand, other laboratory studies as those of Pizek et al. (2007) and Martín-Vide and Prió (2005), are focused on the backwater effect generated by the deck under different submergence conditions.

The capabilities of current 2D river flow models avoid the need of including empirical contraction and expansion coefficients, since the 2D flow patterns generated by the bridge opening and piers can be directly resolved by the model (Costabile et al., 2014, 2015; Mateo-Lázaro et al., 2020). Thus, the main problem when including bridges in a 2D model is how to include the effect of the deck on the flow. There are, at least, 3 possible flow conditions that can occur. If the water depth does not reach the deck, the water surface remains unconstrained, and the shallow water equations give a reasonable approximation of the flow field. If the water depth reaches the lower chord of the deck but not the higher chord, all the water flows under the bridge under pressurised conditions, and the shallow water equations cannot be applied directly. The last possibility is that the water depth exceeds the higher chord of the deck. In such an extreme case, part of the water flows under the deck under pressurised conditions, while the remaining discharge flows over the deck under free surface conditions. Having these 3 possible situations in mind, there are two main approaches that have been used in previous studies to cope with submerged or partially submerged bridges in 2D shallow water models.

The most extended approach is to model the effect of the deck with empirical one-dimensional discharge equations (or rating curves) that relate the head loss to the water discharge through the bridge, as those mentioned previously and presented in experimental studies as Brunner (2010), Hunt (1995), Martín-Vide and Prió (2005), Pizek et al. (2007), Seckin et al. (2007) and Shearman et al. (1986). We include in this approach methods that model the bridge as a local head loss coefficient, as it is done in Ratia et al. (2014), since they are conceptually similar and based on a direct empirical relation between the head loss through the bridge

and the discharge. In this kind of methods, the bridge deck is modeled as an internal condition that is applied over a line of the computational mesh, neglecting the width of the bridge in the streamwise direction. For this reason, in this work we will refer to this approach as Internal Condition for Bridges (ICB), even though some authors call it Internal Boundary Conditions. In our opinion, the term *Internal Boundary* is confusing, since *boundary* conditions are applied at the mesh boundaries, while *internal* conditions are applied at internal lines of the mesh. The empirical equations that are used at these internal conditions depend on one or several coefficients, whose value depends on the geometry of the deck and on the upstream and downstream water levels (relative submergence). The ICB is one of the two approaches used in this study to model the effect of bridges in 2D shallow water models.

A more recent, and much less common, approach to model the pressurised flow under a deck is to modify the standard 2D shallow water equations by adding additional terms that account for the vertical confinement of the flow (Cea and López-Núñez, 2021; Dazzi, 2016; Maranzoni and Mignosa, 2018). This method, which is the second approach used in this study, does not rely on empirical discharge coefficients. The main drawback of this approach is that, up to now, the formulations that have been proposed in the literature cannot account for bridge overtopping, but only for pressurised flow under the bridge deck.

All the previous studies have contributed to the development, calibration and validation of different empirical equations and numerical methods to estimate the backwater effects generated by bridges. However, despite the relevance of bridge modelling in the numerical results of 2D shallow water models, there are few published studies that compare the performance of the mentioned modelling approaches, implemented in 2D models, against laboratory data including partially- and fully-submerged conditions. One of the few studies dealing with the modelling of bridges in 2D shallow water models is the work of Ratia et al. (2014), who presented a set of experiments performed in a 24 cm x 16 cm rectangular cross-section flume, in which the head loss generated by different bridge geometries was measured. The experimental results were used to calibrate and validate a novel head loss formulation to include bridges in shallow water models. The experiments of Ratia et al. (2014) were later on used in several numerical studies as those of Maranzoni et al. (2015), Maranzoni and Mignosa (2018) and Cea and López-Núñez (2021). More recently, Dazzi et al. (2020) used internal

conditions in a 2D shallow water model to account for the effect of bridges, and validated their model against some of the laboratory results presented in Brown (1985), Picek et al. (2007) and Ratia et al. (2014).

In this paper we present a new experimental data set related to flow through bridges. Several tests were conducted in a 15 m long flume with a 50 cm width rectangular cross-section, over 4 different bridge geometries, including simple and multiple circular arches and a rectangular deck with multiple piers. For each bridge geometry, several flow conditions were tested, including free surface, partially-pressurised, fully-pressurised, and overtopped conditions. In all, 32 experimental tests were performed, in which the water depth was measured in a horizontal grid of approximately 110 control points. Thus, the experimental data can be used not only to analyse the total head loss generated by the bridge, as it was usually done in previous studies, but also the detailed 2D water depth pattern created by the piers and deck. This makes it especially suitable to analyse the performance of 2D hydraulic models. All the experimental tests were reproduced with a 2D shallow water model, using two different approaches to account for the deck: the commonly used internal condition for bridges (ICB) and the more recent extension of the Two-component Pressure Approach (TPA) applied by Cea and López-Núñez (2021) to account for the vertical confinement of the flow in the 2D shallow water equations. The ICB approach was first applied using default values of the discharge coefficients included in this method, and then with manually calibrated coefficients obtained from the comparison of the numerical and experimental results. The results obtained with both methods were analysed in terms of the accuracy on the prediction of the headwater depth for a wide range of flow conditions, which is the most important variable in flood inundation studies. Numerical-experimental comparisons of 2D water depth maps around the bridge were also performed.

Experimental tests

The experimental tests were carried out in the open flume of the Civil Engineering School at the University of A Coruña (Spain). The flume is made of steel and methacrylate, it has a length of 15 meters and a rectangular cross-section of 0.5 x 0.5 meters. Its hydraulic circuit can provide a maximum discharge of 50 l/s. At the end

of the flume the water level is controlled with a sluice gate. The bed slope was horizontal in all the tests performed.

Four bridge geometries were tested under different steady flow conditions (Fig. 1). The geometries tested include two simple arch bridges (geometries S1 and S3), a double arch bridge (geometry S2) and a beam bridge (geometry S4). The difference between the two simple arch bridges is that in geometry S1 the arch is centered in the flume cross section and has a diameter of 300 mm, while in geometry S3 the arch has a diameter of 150 mm and it is not aligned with the centerline of the cross section. The high chord of the deck varies between 175 mm and 250 mm, depending on the geometry. In the three arch bridges (geometries S1, S2 and S3), the flow starts to be partially pressurised when the water depth reaches 50 mm, and becomes fully pressurised for water depths of 200 mm in geometry S1 and 125 mm in geometries S2 and S3. Regarding the beam bridge, since the deck is horizontal, there is a direct transition from free surface conditions to fully pressurised conditions. The bridge that produces the highest blockage ratio is S3, while S4 is the one with the lowest blockage.

In all, 32 experimental tests were performed, in which the 4 bridge geometries were tested for a range of discharges ranging from 11 l/s to 48 l/s (10 flow conditions for geometry S1, 7 flow conditions for geometries S2 and S4, and 7 flow conditions for geometry S3). All the tests were performed under steady flow conditions. The downstream boundary condition was established for each test in order to generate different flow conditions at the bridge section, including: free flow, partially pressurised, fully pressurised and overtopped (Fig. 2). The detailed flow conditions for each test are shown in Table 1.

The water depth was measured with an automatic positioner on a grid of points covering a distance of approximately 1200 mm around the bridge (Fig. 2). The number of points in the measurement grid was 117 in all the test cases, except in those with overtopped flow conditions (S2-T05 to S2-T07, and S3-T05 to S3-T08 in Table 1), in which some additional experimental points were located over the bridge deck, achieving a total number of 143 data poins in those cases. The automatic positioner moves a hydraulic piston in the X- and Y-axis, while at the same time the piston moves up and down in the Z-axis uninterruptedly. The piston has two needles attached. When the water surface contacts the needles, an electrical circuit is closed and the water

surface elevation is registered. The coordinates of the needles that measure the water surface elevation are registered with an accuracy of 0.5 mm in the 3 spatial directions.

Since the water surface elevation oscillates in time, a number of independent water depth measurements were taken at each grid point, in order to estimate the average water depth at that location. The number of measurements was increased at the grid points with high turbulence and water depth oscillations. The criterion used to determine the number of independent measurements was that, at each grid point, the standard deviation of the water depth measurements divided by the square root of the number of measurements, was lower than 1 mm. In any case, a minimum number of at least 10 independent measurements were sampled at each grid point.

For each experimental test, two characteristic water depths were defined as the average of the grid points located at the most downstream and at the most upstream rows of the measurement grid (Fig. 2), which will be referred to as h_D and h_U respectively. These values will be used to characterise the experimental conditions of each test (Table 1), as well as to assess the global performance of the numerical model. The upstream depth h_U is of special relevance in flood studies, since it determines the extension of the inundation upstream from the bridge and the profile of the corresponding backwater curve. Considering the experimental configuration and the number of measurements used to compute the average water depth at each control point, the uncertainty in the experimental values of h_D and h_U was estimated to be less than 1 mm.

Numerical model

Hydrodynamic equations

The hydrodynamic model used in this work is the software Iber (Bladé et al. 2014), which solves the 2D depth-averaged shallow water equations (2D-SWE) incuding several turbulence models. In this work we have used the depth-averaged $k-\varepsilon$ model of Rastogi and Rodi (Rodi, 2000). Some simulations were also done using a simpler depth-averaged mixing length turbulence model (Cea et al. 2007), without any relevant differences in the results, which suggests that the potential errors introduced by the turbulence model used in this case are not so relevant as those due to the simplified modelling of the bridge structures.

The shallow water equations are solved with an explicit unstructured finite volume solver, including several schemes for the discretisation of the convective fluxes. In this work we have used a high-order Godunov type scheme based on Roe's approximate Riemann solver (LeVeque, 2002; Toro, 2001). Mathematical details about the discretisation schemes implemented in the model have been published in several previous papers and are therefore not reproduced here. The reader is referred to Bladé et al. (2014), Cea and Bladé (2015) and Cea and Vázquez-Cendón (2012) for a detailed description of the numerical schemes implemented in the solver.

Internal Condition for Bridges (ICB)

The most common approach to include the effect of bridge decks in the 2D-SWE is through the implementation of internal conditions. Internal conditions are defined at specific edges of the computational mesh, which must be aligned with the axis of the bridge deck. The water discharge through the mesh edges that belong to the internal condition is not computed using the standard discretisation of the 2D-SWE, but instead it is computed from an empirical relation that depends on the hydrodynamic variables at some reference points located upstream and downstream from the edge (Fig. S1 of the Supplemental Material). Different empirical equations and implementations have been used for that purpose in previous studies (Bladé et al. 2014; Dazzi et al. 2020; Ratia et al. 2014). The implementation used in this work is described in detail in the Supplemental Material.

Two-component Pressure Approach (TPA)

An alternative approach to include the effect of a deck in the flow is to modify the 2D-SWE in order to account for the vertical confinement of the water under the deck. Two methodologies have been proposed in the last years to model mixed free-surface-pressurised conditions with the 2D-SWE: the Preissmann Slot Model (Maranzoni et al. 2015; Maranzoni and Mignosa, 2018) and the Two-component Pressure Approach (Cea and López-Núñez, 2021). Both methods were developed as an extension of the standard 2D-SWE, and their application to a bridge deck is limited to free surface or pressurised conditions, not being possible to model overflow conditions over the deck. In this study we have used the TPA extension of the 2D-SWE, which is limited to non-overtopping flow conditions. A detailed mathematical description of the method is given by Cea and López-Núñez (2021), while the most relevant aspects of its numerical implementation are included in the Supplemental Material.

Results and discussion

Model setup

Although the length of the experimental flume is 15 m, only a section of 5.2 m was included in the numerical models, since the flow outside from this section was rather uniform. The outlet boundary was located at the same section at which the water depth was measured with a limnimiter in the experiments, in order to fix a correct value of the boundary condition in the numerical model. The bridges were located approximately 2 m upstream from that boundary (Fig. 3). The inlet boundary was located approximately 3 m upstream from the bridge.

Due to the relatively simple geometry of the experimental flume, a structured mesh with 5600 elements was used in all the numerical simulations, with a uniform mesh size in all the domain except in a region of 1.2 m around the bridge, where the mesh was refined to have 20 mesh elements of 2.5 cm across the bridge cross section. This discretisation was chosen after a mesh convergence analysis detailed in the Supplemental Material.

In order to establish the deck elevation used in the ICB equations, the shape of the arch bridges was discretised in several steps of constant elevation, as shown in Fig. 4. In this way, the elevation of the low chord of the deck varies along the line that defines the internal condition. The rest of coefficients in the ICB equations ($C_{g,1}$, $C_{g,2}$ and C_w) have the same value all along the internal condition.

The numerical simulations with the TPA approach were performed using a computational mesh with the same spatial resolution as the one used in the ICB approach. The main difference is that the low chord elevation is defined at the mesh elements (instead of mesh edges) and therefore, the width of the deck in the streamwise direction is not neglected (Fig. 5). The discretisation of the bridge cross section was the same as in the ICB approach (Fig. 4). The value of the stiffness constant was set to $K_r = 100$ m/s^2, after a numerical convergence analysis detailed in the Supplemental Material.

Headwater results

For practical purposes in river inundation modelling, the most important result that can be obtained from the experimental tests is the water surface elevation upstream from the bridge, since it will determine the elevation of the backwater curve and thus, the extension of the flood. Fig. 6 shows the experimental and numerical water depths at a control point located 40 cm upstream from the bridge, computed with the ICB and TPA methods. As mentioned in section 3.3, the application of the TPA method is limited to those cases with no overflow over the deck. This implies that some of the flow conditions tested in the geometries S2 and S3 could not be modelled with TPA. Those were the test cases S2-T05 to S2-T07 in geometry S2 and S3-T05 to S3-T08 in geometry S3 (Table 1). In all, 25 test cases were modelled with the TPA approach.

The ICB numerical results were computed with the default coefficients included in the software Iber for the discharge equations in Table S1 and Table S2 of the Supplemental Material (Bladé et al., 2014), which are those recommended by Brunner (2010). In the case of the TPA method, there are no coefficients to calibrate other than the stiffness constant, which is not really a calibration parameter, but rather a numerical stability parameter. This means that no specific parameter calibration against observed data was done for these results and thus, Fig. 6 represents the expected experimental-numerical agreement when no calibration data is available.

In order to characterise the numerical-experimental agreement in the ensemble of the experimental tests, we computed the mean absolute error (MAE) and the mean relative absolute error (MRAE) for each numerical approach, defined as:

$$MAE = \frac{1}{N}\sum_{i=1}^{N}\left|h_{U,i}^{num} - h_{U,i}^{exp}\right| \qquad MRAE = \frac{1}{N}\sum_{i=1}^{N}\frac{\left|h_{U,i}^{num} - h_{U,i}^{exp}\right|}{h_{U,i}^{exp}} \tag{7}$$

where N is the number of experimental test cases presented in Table 1 and $h_{U,i}^{num}$ and $h_{U,i}^{exp}$ are the upstream water depths computed with the numerical model measured in the laboratory respectively. The MAE obtained with the TPA and ICB methods are 2.8 and 11.3 mm respectively, while the MRAE are 0.018 and 0.066.

Considering each individual test case, there is a certain trend in the numerical error, that tends to increase as the water depth increases, especially in the ICB approach and to a much lower degree in the TPA method (Fig. 6). This could be expected, since when the water depth is low the bridges are under free or partially submerged

conditions and thus, the influence on the results of the method used to model the deck is lower. Nonetheless, it is interesting to notice that the TPA method reproduces very accurately the observed data in all the range of water depths, while the ICB approach overestimates the upstream water depth in almost all the cases.

In order to improve the agreement with the observed data, the discharge coefficients included in the ICB formulations ($C_{g,1}, C_{g,2}, C_w$) were manually calibrated. No specially procedure was used for the calibration, other than using the same coefficients for all the experimental geometries and tests. This means that the coefficients were calibrated for the ensemble of bridge geometries and flow conditions, and not for each test or geometry independently. Since the numerical results overestimate the experimental data, the value of all the discharge coefficients was progressively increased until the MAE was reduced to a minimum, which was achieved for $C_{g,1} = 0.8, C_{g,2} = 1.0$ and $C_w = 2.1$. With these coefficients, the ICB results fit much better the observations, as shown in Fig. 7, and the MAE is reduced to 4.3 mm. Moreover, if we just consider the experimental tests with no overtopping (as indicated in Table 1), which are those that have been modelled with the TPA method, the MAE is further reduced to 4.1 mm. The numerical-experimental differences are much lower than those obtained with the default coefficients, but still larger than those obtained with TPA.

The calibrated discharge coefficients are rather high compared to their default value, especially the weir discharge coefficient, with a value equivalent to that of a sharp-crested weir. This is probably due to the experimental setup. Even if the bridges have a realistic geometry, the absence of imperfections, hand rails or balustrades, might have a positive effect on their discharge capacity. Under field conditions, the discharge coefficients would probably be lower.

In order to transform the results to the field scale, it can be considered that the scale of the bridge models used in the experiments is something between 1:20 and 1:40. At those spatial scales, assuming the Froude similarity, the width of the channel would be between 10 and 20 m, the height of the bridges between 3.5 m and 10 m (depending on the bridge geometry), and the upstream water depth for the different flow conditions between 1.6 m and 10 m. River discharges would be roughly between 20 m^3/s and 500 m^3/s. Those values cover a wide range of realistic conditions. For those spatial scales, the MAE of the TPA method would be between 5.6 and 11 cm, which are quite low errors for real scale conditions. Regarding the ICB approach, the

MAE would be between 22.5 and 45 cm when using the default discharge coefficients, which are rather high values. However, after the manual calibration, the MAE would be reduced to something between 8.5 and 17 cm, which is much more acceptable for practical purposes.

Two-dimensional water depth maps

An added value of the experimental results presented in this work with respect to other studies on bridge hydraulics, is the characterisation of the water depth spatial patterns around the bridges. While the headwater depth is the most relevant variable for inundation studies, the characterisation of the spatial flow pattern around the bridge is important because it has an impact on the local scour. Although the experimental data presented here does not include flow velocities, the 2D water depth maps can be used as a first verification in order to evaluate to what extent a numerical model is able to reproduce the local flow patterns. This is known to be a weakness of shallow water models, because the two main shallow water assumptions (i.e. quasi-hydrostatic pressure and absence of vertical velocity gradients) are broken due to the 3D velocity field generated nearby hydraulic structures. In this sense, a good representation of the water depth pattern is a necessary (but not sufficient) condition to reproduce the water velocity.

In all the test cases defined in Table 1, the water depth was measured in a spatial grid of around 120 and 140 locations, depending on the bridge geometry. All the experimental data can be found in the following repository https://zenodo.org/record/5040729#.YNsff0ztZPY. For the sake of conciseness, only some relevant figures are shown in the following.

In general, both the TPA and ICB approaches are able to reproduce the water depth patterns under free surface or very slightly partially-pressurised conditions, as well as for completely submerged conditions, because in these cases the water depth is rather uniform upstream and downstream from the bridge. This is the case, for instance, of tests S1-T08 in Fig. 8, S2-T01 in Fig. 9, S3-T03 in Fig. 10 and S4-T07 in Fig. 11. Nevertheless, as mentioned above, this does not guarantee a proper representation of the water velocities, since there might be 2D recirculation patterns generated downstream the piers that are not reflected on the water depth. For instance, the experimental data on the test S2-T01 in Fig. 9 shows a small water depth disturbance generated by the pier that separates the two bridge arches, which is generated by the stagnant

region located in the downstream face of the pier. This spatial pattern is not reproduced by the numerical model.

The experimental-numerical disagreement is larger in the partially submerged tests. In these cases, the spatial variability of the water surface is much larger, and there might even be hydraulic jumps that are not captured by the numerical model, as for instance in the tests S1-T10 in Fig. 8, S2-T04 in Fig. 9 and S4-T06 in Fig. 11. The water velocity computed by the model in these cases is probably very different from the real one, a 3D model being necessary for a better representation of the spatial flow patterns.

Fig. 12 shows the longitudinal profile of the water depth along the center line of the flume in some representative test cases. Again, it can be observed that the headwater depth is rather well captured by the models, while some differences appear in the local water depth just downstream from the bridge, specially with the ICB approach. The TPA method is able to capture the trends in the water depth, but in general it fails to give an accurate prediction of the local water depth just downstream the bridge, with the exception of the cases in which the water depth is rather uniform upstream and downstream from the bridge.

It is also interesting to notice that, even if the TPA method showed a better capability than the ICB approach to capture the experimental headwater depth, as shown in Fig. 6 and Fig. 7, regarding the representation of the local flow patterns both approaches show the same limitations. The mean absolute error (MAE) computed from the difference between the experimental data and the numerical predictions at all the observation points is very similar regardless the method used to model the bridge (Fig. 13). This is because these numerical inaccuracies arise mainly from the shallow water assumptions, which are common to both methods. On the other hand, the MAE is very sensitive to the flume discharge in all the geometries.

The MAE varies roughly between 2 mm and 25 mm, depending on the flow conditions and on the bridge geometry. In all the cases modelled with the TPA method (those with no overtopping), the MAE is always lower than 10 mm except in the case of S1-T10, where it reaches almost 15 mm. Assuming a spatial scale between 1:20 and 1:40 in our experiments, in a real river reach these values would translate to average errors between 20 and 50 cm, which are rather large. If we consider the whole experimental data set, the MAE even

reaches, under certain conditions, values larger than 20 mm. This is the case of tests S2-T05, S2-T06, S3-T05 and S3-T07 (Fig. 13), all of them with overtopping conditions.

Conclusions

Two different methods for including the effect of bridges in 2D shallow water models have been tested and compared in 4 different bridge geometries and different flow conditions. For this purpose, the headwater depth, as well as the spatial distribution of water depth, was measured in 32 experimental tests in a laboratory flume. The experimental data can be used to analyse the head loss generated by the bridge, as well as to test different numerical approaches and models of water flow through bridges.

The TPA method showed a very good global performance regarding the estimation of the headwater depth, without the need of any calibration parameter. On the other hand, the ICB approach overestimated the observed headwater depth when used with the default value of the discharge coefficients. However, after a relatively simple manual calibration, the ICB method was able to reproduce much better the upstream water surface elevation observed in the experiments. This means that, when no calibration data is available, it is advisable to use the TPA method, while both methods might be adequate after a proper calibration and validation with observed data.

Assuming a spatial scale of 1:20 in our laboratory experiments (i.e. a bridge of approximately 3 m height and 10 m width), the MAE in the headwater depth, considering all the experimental tests, would be around 5 cm for the TPA and 8 cm for the ICB method after a manual calibration of the ICB coefficients. On the other hand, under the same conditions the MAE with the ICB approach using the default discharge coefficients increases to 22 cm. Nevertheless, the calibrated values of the ICB coefficients obtained in this work might not be adequate for real conditions, since there might be other features as irregularities on the geometry or the existence of hand rails, that can have an effect on the discharge capacity of the bridge.

Regarding the 2D water depth patterns, both methods showed the same limitations, as it could be expected from the fact that the basic shallow water assumptions are broken under many of the flow conditions that were used in the experimental tests. The MAE on the spatial patterns of water depth around the bridge varies

between 2 mm for the lowest discharges (around 10 l/s) up to 25 mm in some test cases with overtopping conditions. Under partially submerged conditions none of the methods is able to reproduce the local spatial patterns on the water surface. On the other hand, under completely submerged or under free surface conditions, the water depth pattern is rather uniform and thus, it is correctly reproduced in the models.

Data Availability Statement

All the experimental data generated during the study are available in a repository online in accordance with funder data retention policies (DOI: 10.5281/zenodo.5040728).

All the numerical models that support the findings of this study are available from the corresponding author upon reasonable request.

Acknowledgements

This study received financial support from the Spanish Ministry of Science, Innovation and Universities (Ministerio de Ciencia Innovacion y Universidades) within the project "VAMONOS: Development of non-hydrostatic models for environmental hydraulics. Two dimensional flow in rivers" (reference CTM2017-85171-C2-2-R).

References

Areu-Rangel, O. S., Cea, L., Bonasia, R., & Espinosa-Echavarria, V. J. (2019). Impact of urban growth and changes in land use on river flood hazard in Villahermosa, Tabasco (Mexico). *Water*, 11(2), 304.

Belaud, G., Cassan, L., Baume, J. P. (2009). Calculation of contraction coefficient under sluice gates and application to discharge measurement. *Journal of Hydraulic Engineering*, 135(12), 1086-1091.

Bermúdez, M., Cea, L., Sopelana, J. (2019). Quantifying the role of individual flood drivers and their correlations in flooding of coastal river reaches. *Stochastic Environmental Research and Risk Assessment*, 33(10), 1851-1861.

Bladé, E., Cea, L., Corestein, G., Escolano, E., Puertas, J., Vázquez-Cendón, E., Dolz, J., Coll, A. (2014). Iber: herramienta de simulación numérica del flujo en ríos. *Rev. Int. Metod. Numer. Calc. Disen. Ing*., 30, 1–10, DOI: 10.1016/j.rimni.2012.07.004

Brown, P.M. (1985). Afflux at British bridges: Interim Report. Hydraulic Research Wallingford, Wallingford, UK Report SR, 60.

Brunner, G. W. (1995). HEC-RAS River Analysis System. Hydraulic Reference Manual. Version 1.0. Hydrologic Engineering Center Davis CA.

Cea, L., Bladé, E. (2015). A simple and efficient unstructured finite volume scheme for solving the shallow water equations in overland flow applications. *Water Resources Research*, 51(7), 5464-5486. DOI: 10.1002/2014WR016547.

Cea, L., López-Núñez, A. (2021). Extension of the two-component pressure approach for modeling mixed free-surface-pressurised flows with the two-dimensional shallow water equations. *International Journal for Numerical Methods in Fluids*, 93(3), 628-652. DOI: 10.1002/fld4902.

Cea, L., Puertas, J., Vázquez-Cendón, M.E. (2007). Depth averaged modelling of turbulent shallow water flow with wet-dry fronts. *Archives of Computational Methods in Engineering*, 14(3), 303-341. DOI: 10.1007/s11831-007-9009-3.

Cea, L., Vázquez-Cendón, M.E. (2012). Unstructured finite volume discretisation of bed friction and convective flux in solute transport models linked to the shallow water equations. *Journal of Computational Physics*, 231(8), 3317–3339.

Clemmens, A. J., Strelkoff, T. S., Replogle, J. A. (2003). Calibration of submerged radial gates. *Journal of Hydraulic Engineering*, 129(9), 680-687.

Costabile, P., Macchione, F., Petaccia, G., Natale, L. (2014). Representing skewed bridge crossing on 1-D and 2-D flood propagation models: compared analysis in practical studies. In Proceedings Int. Conf. on fluvial hydraulics river flow, 733-741.

Costabile, P., Macchione, F. (2015). Enhancing river model set-up for 2-D dynamic flood modelling. *Environmental Modelling & Software*, 67, 89-107.

Costabile, P., Macchione, F., Natale, L., Petaccia, G. (2015). Comparison of scenarios with and without bridges and analysis of backwater effect in 1-D and 2-D river flood modeling. *Comput Modell Eng Sci*, 109(2), 181-204.

Dazzi, S. Numerical modelling of unsteady mixed flow. PhD Thesis. 2016

Dazzi, S., Vacondio, R., Mignosa, P. (2020). Internal boundary conditions for a GPU-accelerated 2D shallow water model: implementation and applications. *Advances in Water Resources*, 137, 103525.

Fraga, I., Cea, L., Puertas, J. (2020). MERLIN: a flood hazard forecasting system for coastal river reaches. *Natural Hazards*, 100(3), 1171–1193. DOI: 10.1007/s11069-020-03855-7.

García-Feal, O., González-Cao, J., Gómez-Gesteira, M., Cea, L., Domínguez, J. M., Formella, A. (2018). An accelerated tool for flood modelling based on Iber. *Water Switz.*, 10, 1–23, DOI:10.3390/w10101459

Garrote, J., Alvarenga, F. M., Díez-Herrero, A. (2016). Quantification of flash flood economic risk using ultra-detailed stage–damage functions and 2-D hydraulic models. *Journal of hydrology*, 541, 611-625.

Hamill, L. (1999). Bridge Hydraulics. E&FN SPON, London, NewYork. ISBN 9780367447632

Hunt, J. H. (1995). Flow transitions in bridge backwater analysis (Vol. 42). US Army Corps of Engineers, Hydrologic Engineering Center.

Hunt, J., Brunner, G. W., Larock, B. E. (1999). Flow transitions in bridge backwater analysis. *Journal of Hydraulic Engineering*, 125(9), 981-983.

LeVeque, R. J., 2002. Finite Volume Methods for Hyperbolic Problems. Cambridge Texts in Applied Mathematics, 31. Cambridge University Press

Maranzoni, A., Dazzi, S., Aureli, F., Mignosa, P. (2015). Extension and application of the Preissmann slot model to 2D transient mixed flows. *Advances in Water Resources,* 82, 70-82.

Maranzoni, A., Mignosa, P. (2018). Numerical treatment of a discontinuous top surface in 2D shallow water mixed flow modeling. *International Journal for Numerical Methods in Fluids*, 86(4), 290-311.

Martin-Vide, J. P., Prio, J. M. (2005). Backwater of arch bridges under free and submerged conditions. *Journal of Hydraulic Research*, 43(5), 515-521.

Mateo-Lázaro, J., Castillo-Mateo, J., García-Gil, A., Sánchez-Navarro, J. Á., Fuertes-Rodríguez, V., Edo-Romero, V. (2020). Comparative Hydrodynamic Analysis by Using Two−Dimensional Models and Application to a New Bridge. *Water*, 12(4), 997.

Montes, J. S. (1997). Irrotational flow and real fluid effects under planar sluice gates. *Journal of Hydraulic Engineering*, 123(3), 219-232.

Ocio, D., Stocker, C., Eraso, Á., Martínez, A., & de Galdeano, J. M. S. (2016). Towards a reliable and cost-efficient flood risk management: the case of the Basque Country (Spain). *Natural Hazards*, 81(1), 617-639.

Picek, T., Havlik, A., Mattas, D., Mares, K. (2007). Hydraulic calculation of bridges at high water stages. *Journal of Hydraulic Research*, 45(3), 400-406.

Ratia, H., Murillo, J., García-Navarro, P. (2014). Numerical modelling of bridges in 2D shallow water flow simulations. *International Journal for Numerical Methods in Fluids,* 75(4), 250-272.

Seckin, G., Haktanir, T., Knight, D. W. (2007). A simple method for estimating flood flow around bridges. In *Proceedings of the Institution of Civil Engineers-Water Management*, 160(4), 195-202. Thomas Telford Ltd.

Shearman, J. O., Kirby, W. H., Schneider, V. R., & Flippo, H. N. (1986). Bridge waterways analysis model (No. FHWA-RD-86-108). United States. Federal Highway Administration.

Swamee, P. K. (1992). Sluice-gate discharge equations. *Journal of Irrigation and Drainage Engineering*, 118(1), 56-60.

Toro, E.F., 2001. Shock-Capturing Methods for Free-Surface Shallow Flows. Wiley, Chichester, West Sussex, England

Table 1. Summary of the experimental tests. Downstream and upstream water depths refer to the average of the points located in the most downstream and most upstream rows of the experimental measurement grid (Fig. 2).

Bridge type	Test	Discharge (l/s)	Water depth (mm)		Flow conditions
			Downstream (h_D)	Upstream (h_U)	
S1 Simple Arch Symmetric	S1-T01	11.25	79.0	88.9	Partially pressurised
	S1-T02	12.11	236.0	238.7	Fully pressurised
	S1-T03	17.43	88.4	109.4	Partially pressurised
	S1-T04	19.09	225.0	231.2	Fully pressurised
	S1-T05	24.46	121.0	134.1	Partially pressurised
	S1-T06	23.68	204.7	212.0	Fully pressurised
	S1-T07	30.70	112.0	156.9	Partially pressurised
	S1-T08	30.45	213.0	229.1	Fully pressurised
	S1-T09	37.72	133.0	175.0	Partially pressurised
	S1-T10	47.60	154.0	219.7	Fully pressurised
S2 Double Arch Symmetric	S2-T01	11.85	74.0	85.5	Partially pressurised
	S2-T02	18.36	91.0	113.6	Partially pressurised
	S2-T03	23.78	101.0	135.2	Partially pressurised
	S2-T04	29.04	117.0	157.1	Fully pressurised
	S2-T05	38.75	133.7	188.1	Overtopped
	S2-T06	48.08	63.4	205.0	Overtopped
	S2-T07	47.96	191.4	220.8	Overtopped
S3 Simple Arch Asymmetric	S3-T01	12.07	80.0	142.7	Partially pressurised
	S3-T02	12.16	116.5	153.3	Partially pressurised
	S3-T03	12.11	126.5	159.7	Fully pressurised
	S3-T04	12.15	141.2	171.8	Fully pressurised
	S3-T05	18.36	94.6	188.7	Overtopped
	S3-T06	19.15	155.3	200.3	Overtopped
	S3-T07	29.9	120.4	222.1	Overtopped
	S3-T08	29.6	197.0	235.6	Overtopped
S4 Beam	S4-T01	11.98	75.0	80.7	Free
	S4-T02	18.12	71.0	87.5	Free
	S4-T03	24.29	89.0	104.5	Free
	S4-T04	32.31	126.0	133.6	Free
	S4-T05	38.84	122.0	138.6	Free
	S4-T06	47.48	132.9	162.3	Fully pressurised
	S4-T07	47.27	156.9	175.7	Fully pressurised

Fig. 1. Geometry of the bridges tested. Dimensions are shown in mm.

Fig. 2. Flow conditions at the bridge section (left, side view) and example of grid of measurement points at which the water depth was measured (right, top view). In the right plot the water flows from right to left.

Fig. 3. Numerical mesh used in the ICB models, with 5600 elements. The deck elevation varies along the internal condition, as shown in Fig. 4.

Fig. 4. Discretisation of the bridges cross section in order to define the low chord elevation of the deck in both the ICB and TPA methods. Units in mm.

Fig. 5. Numerical discretisation of geometry S1 (simple arch bridge) used in the TPA approach. The element sizes are 2.5 cm^2 in the refined mesh region and 6.25 cm^2 in the rest of the flume.

Fig. 6. Experimental vs. numerical water depth at a control point located 40 cm upstream from the bridge, using the TPA (left) and ICB (right) approaches. Numerical results obtained with the default values of the discharge coefficients ($C_{g,1} = 0.6, C_{g,2} = 0.8$ and $C_w = 1.7$).

Fig. 7. Experimental vs. numerical water depth at a control point located 40 cm upstream from the bridge, using the ICB approach after calibration of the discharge coefficients ($C_{g,1} = 0.8, C_{g,2} = 1.0$ and $C_w = 2.1$). Experimental tests with no overtopping (left) and all experimental tests (right).

Fig. 8. Three dimensional representation of the water surface elevation observed and computed for the experimental cases S1-T08 and S1-T10.

Fig. 9. Three dimensional representation of the water surface elevation observed and computed for the experimental cases S2-T01 and S2-T04.

Fig. 10. Three dimensional representation of the water surface elevation observed and computed for the experimental cases S3-T01 and S3-T03.

Fig. 11. Three dimensional representation of the water surface elevation observed and computed for the test cases S4-T06 and S4-T07.

Fig. 12. Longitudinal profiles along the center line of the flume of the observed and computed water depth for some representative test cases.

Fig. 13. Mean Absolute Error (MAE) in the 2D water depth maps, for all the experimental tests computed with the TPA and ICB methods.

Fig 1

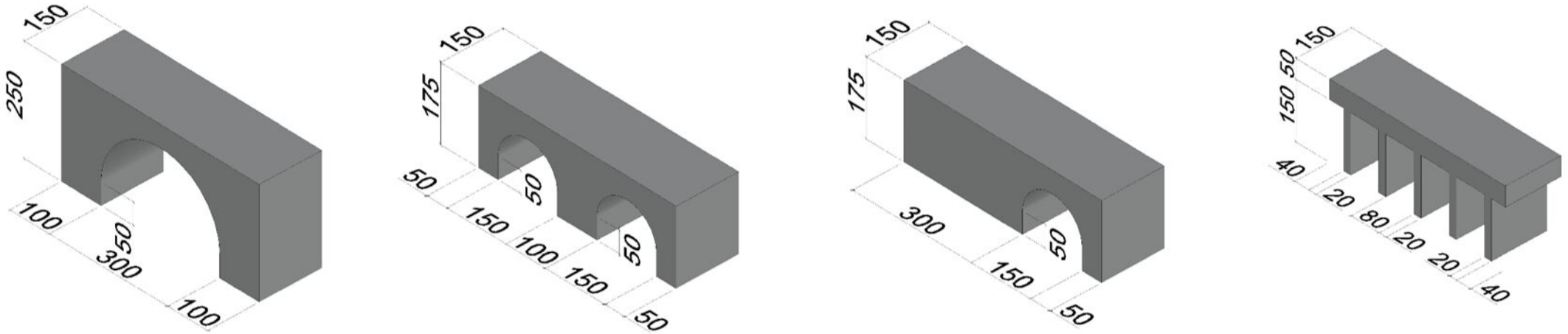

S1 - Simple arch bridge

S2 - Double arch bridge

S3 - Asymmetric arch bridge

S4 - Beam bridge

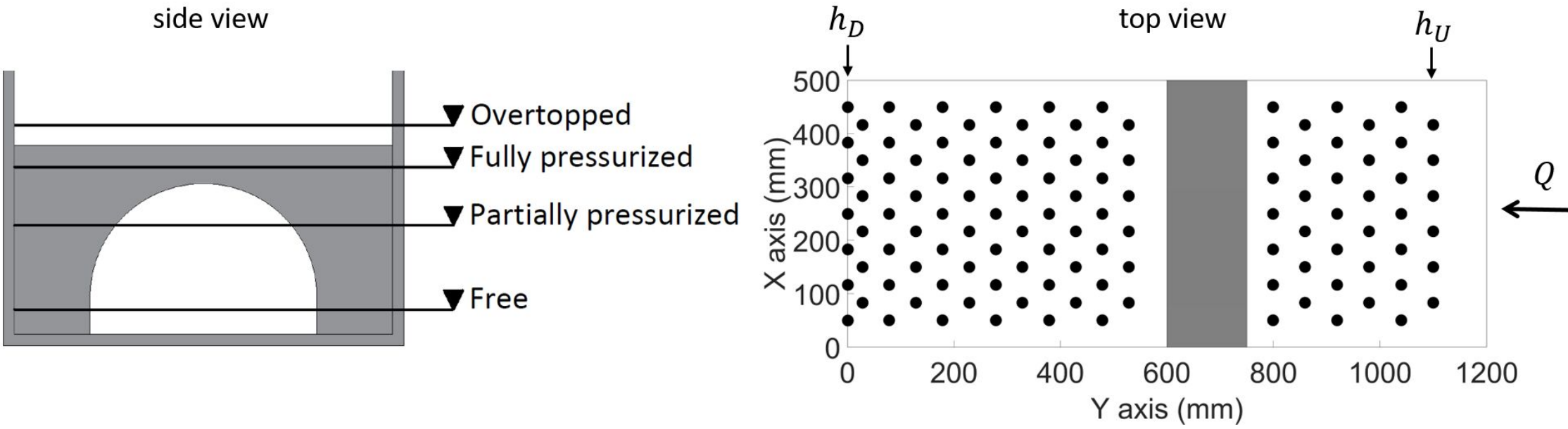

Fig 3

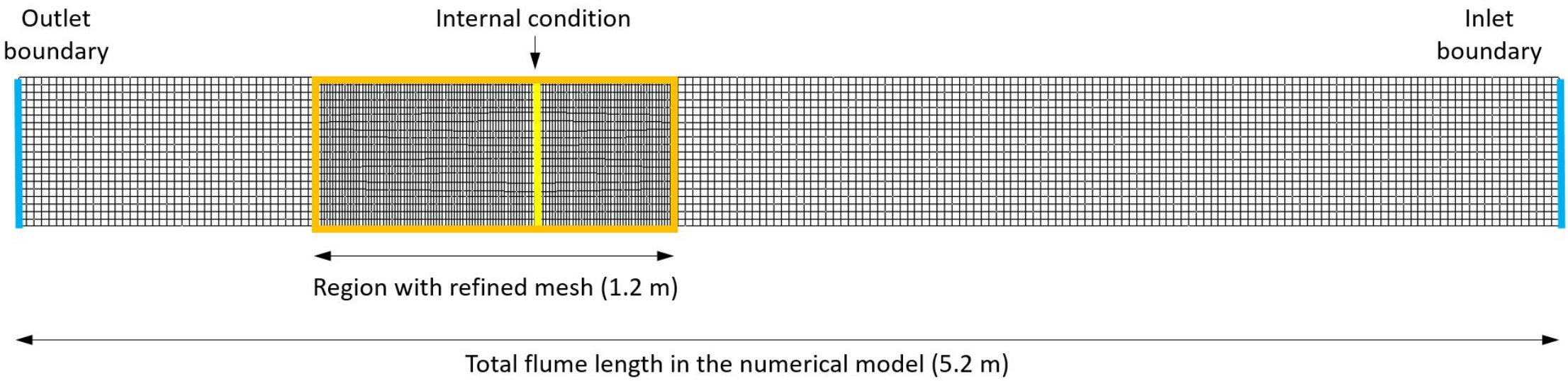

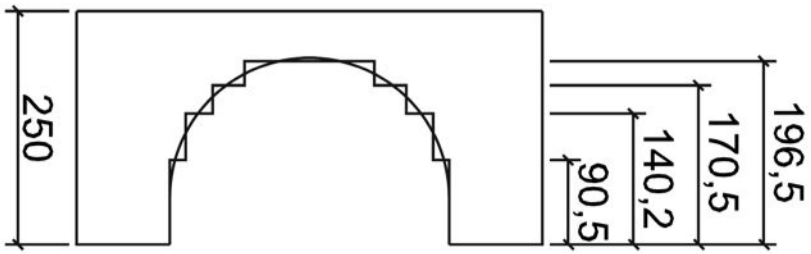

S1 – Simple arch bridge

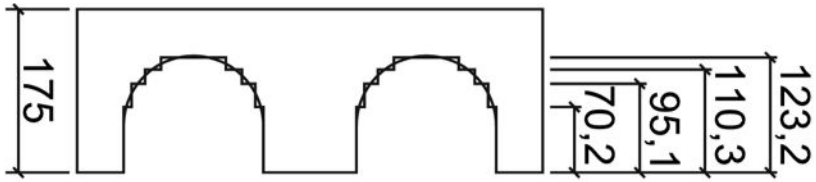

S2 – Double arch bridge

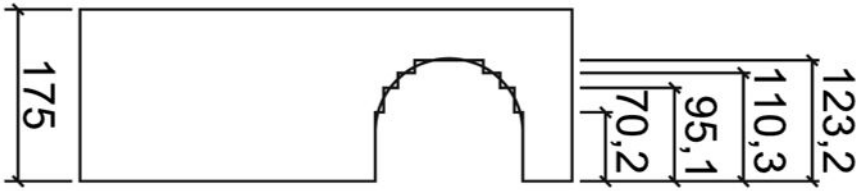

S3 – Asymmetric arch bridge

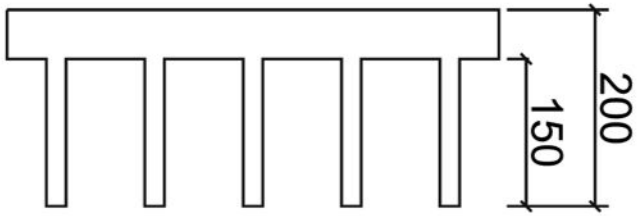

S4 – Beam bridge

Fig 5

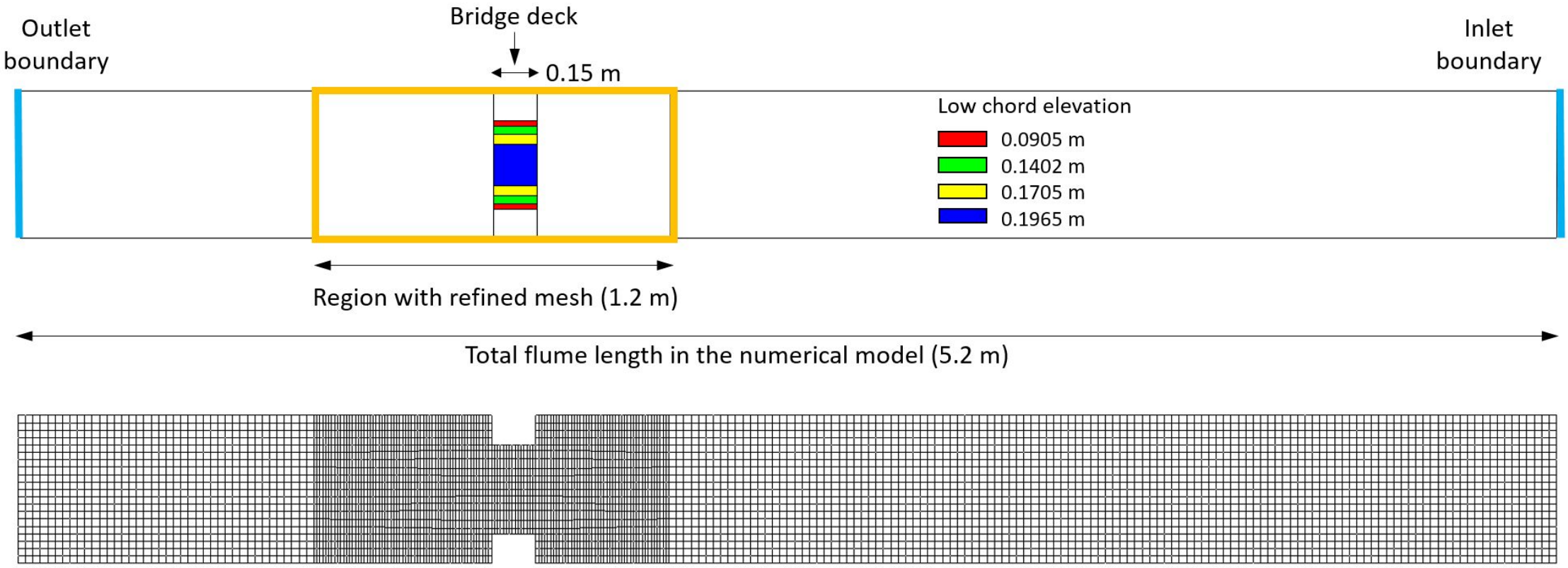

Fig 6

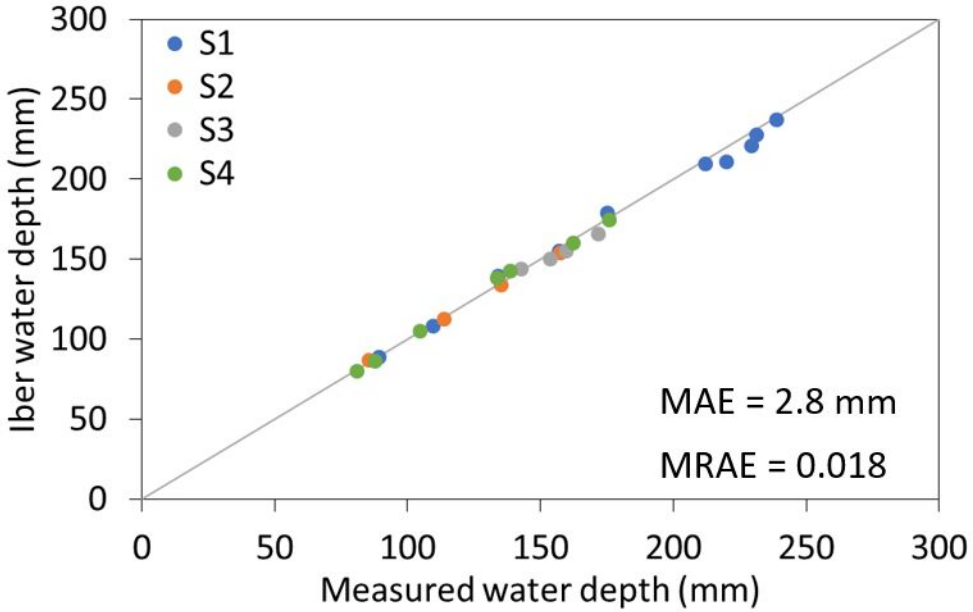

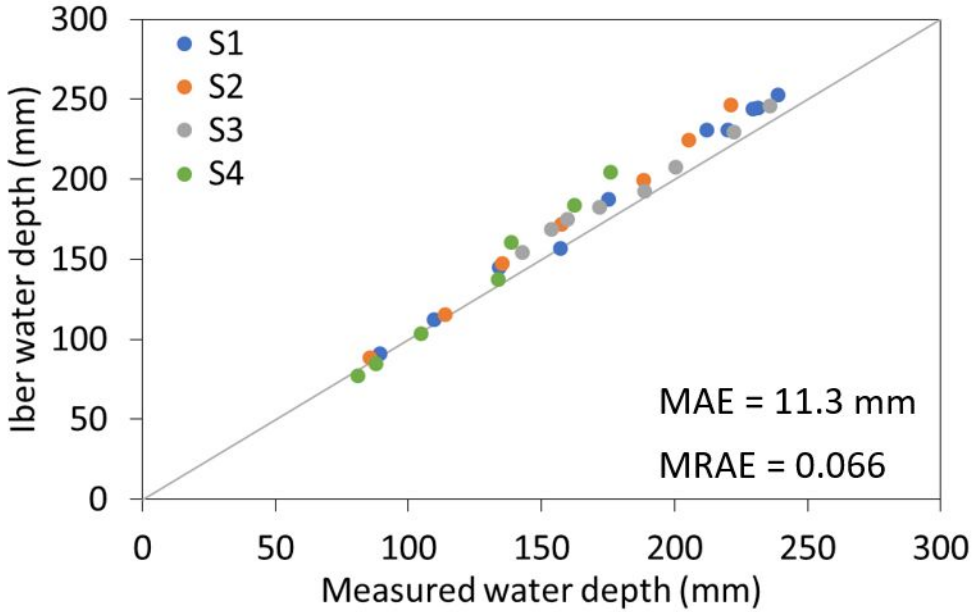

Fig 7

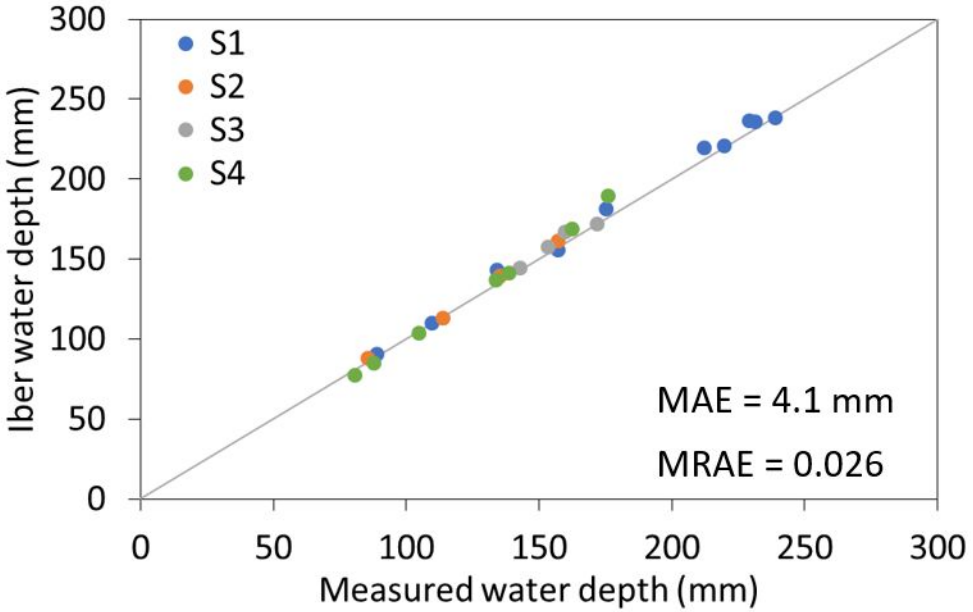

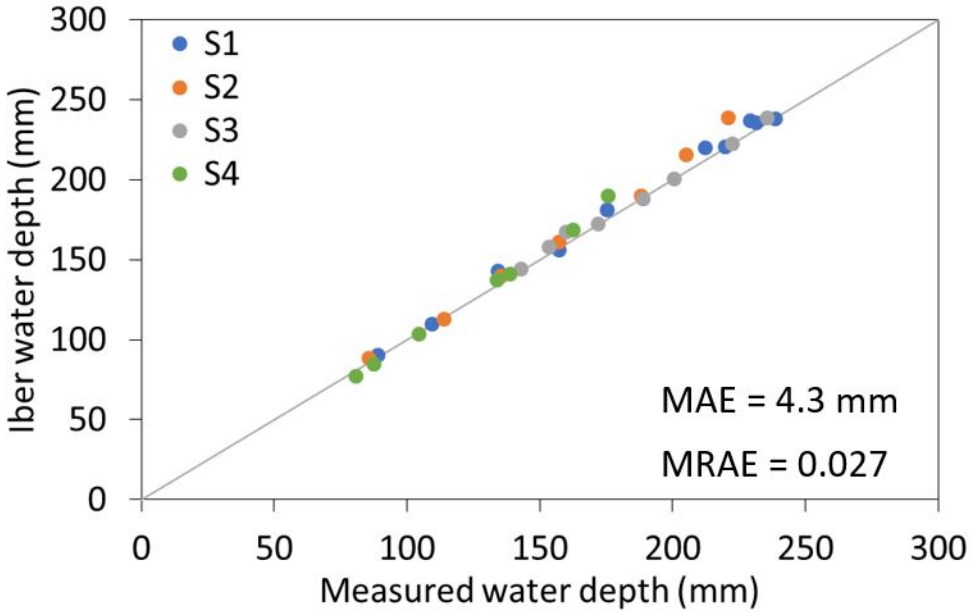

Fig 8

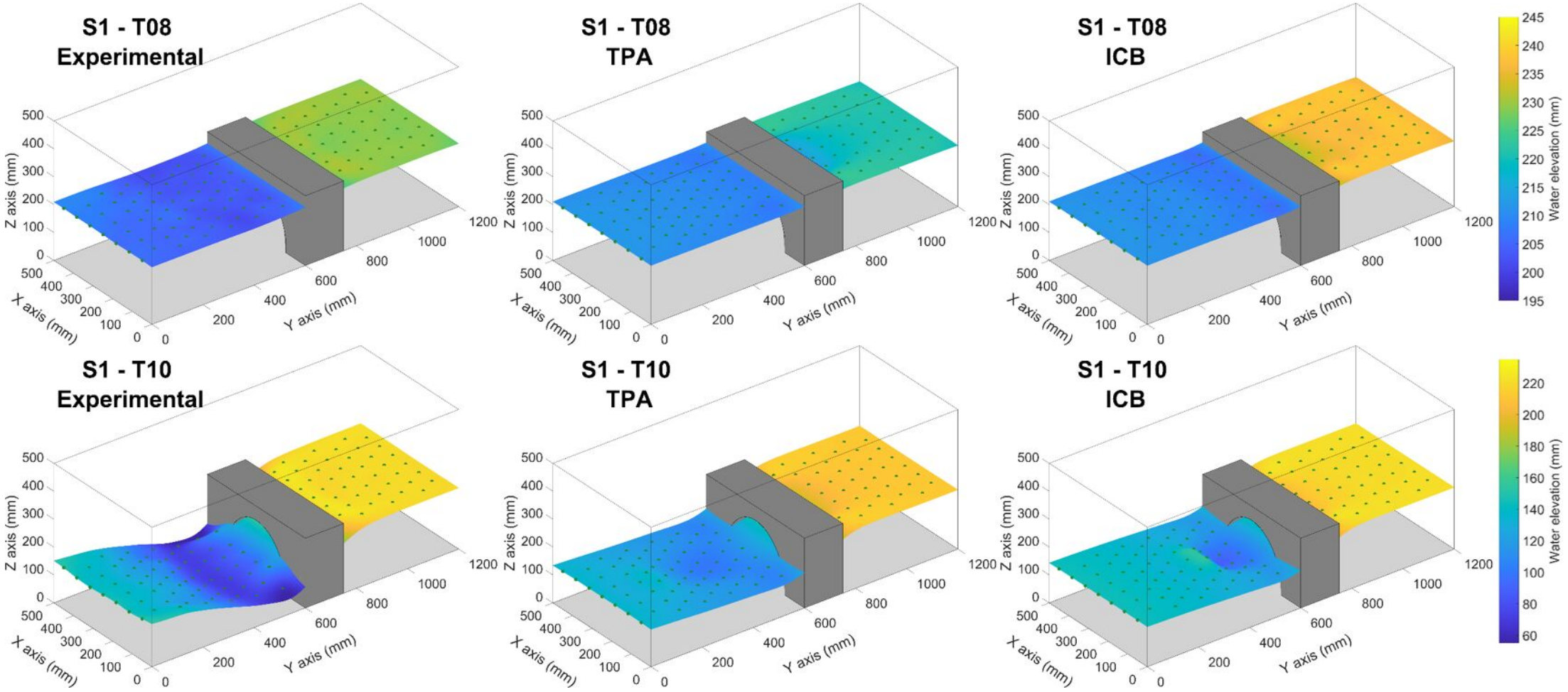

Fig 9

Click here to access/download;Figure;Figure9.pdf

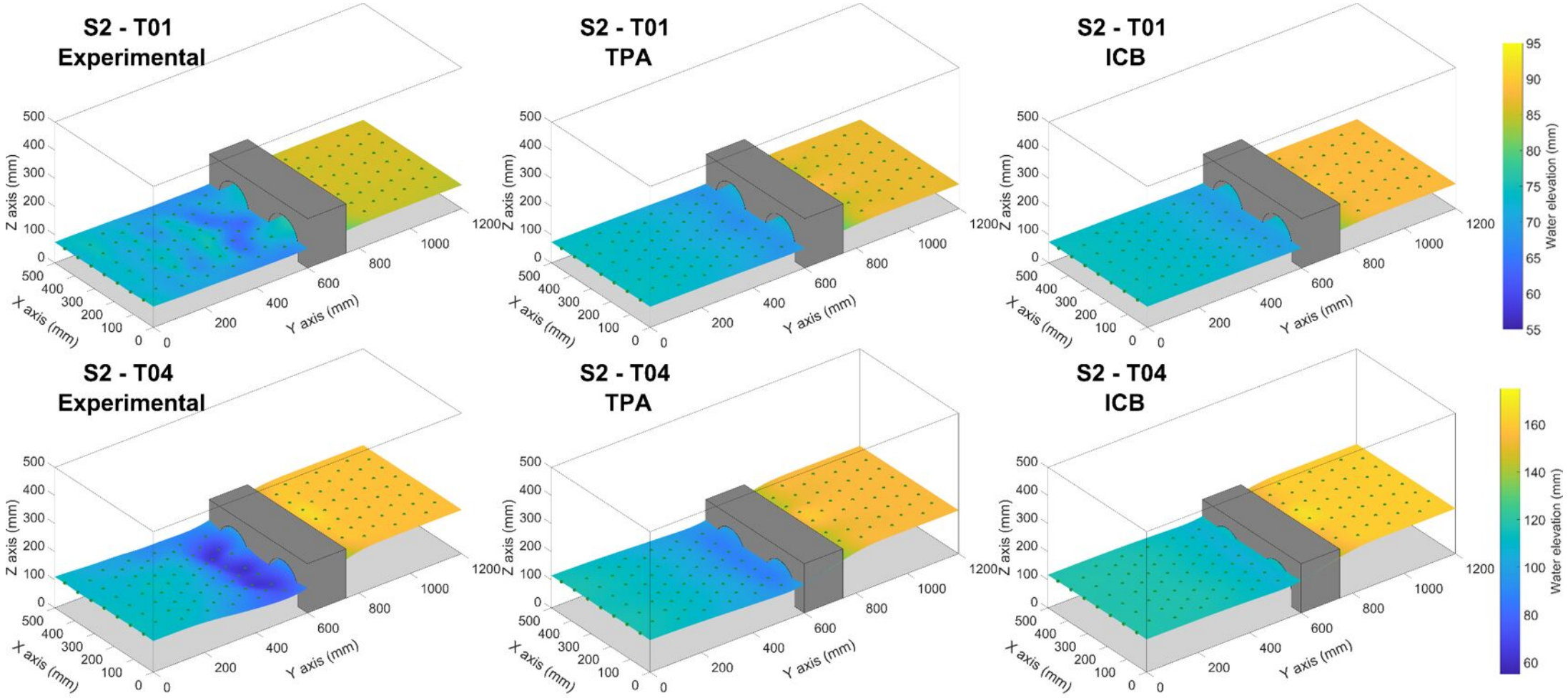

Fig 10

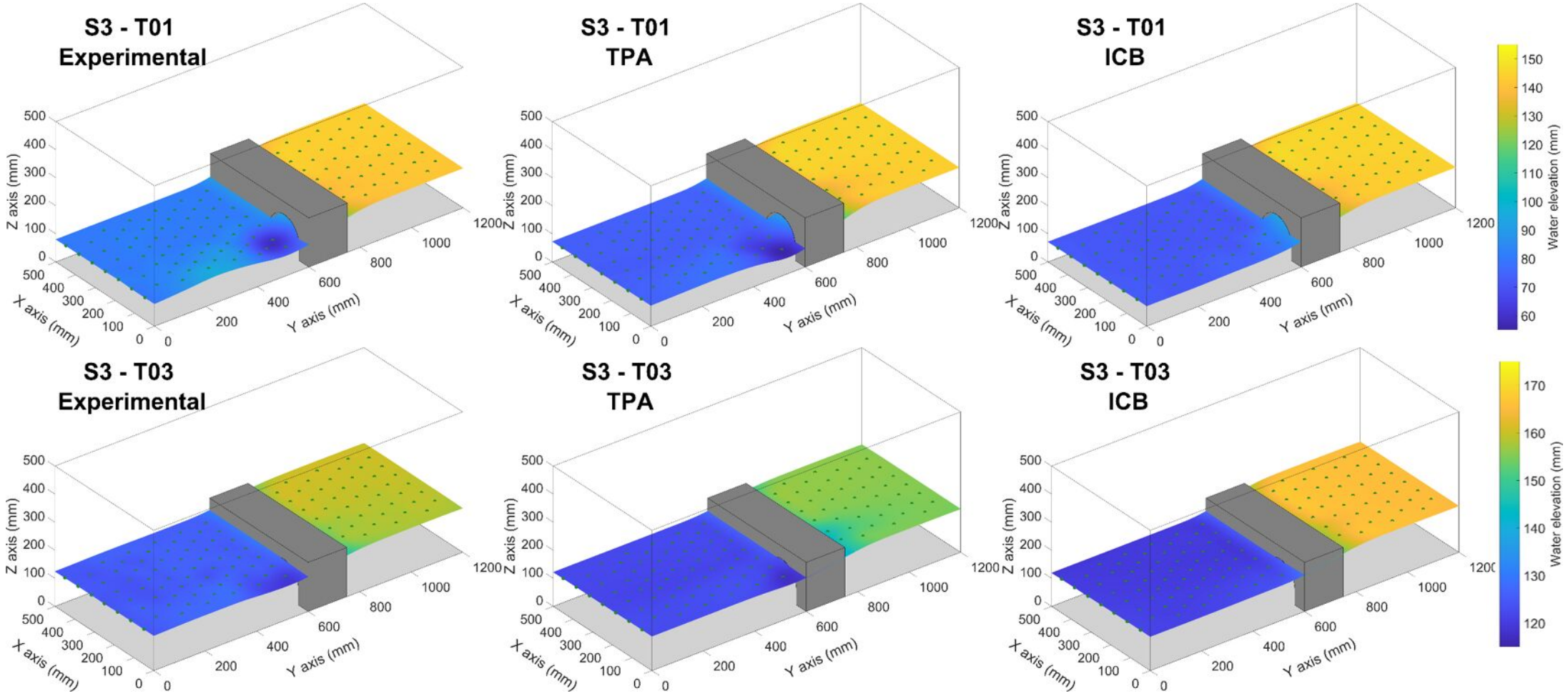

Fig 11

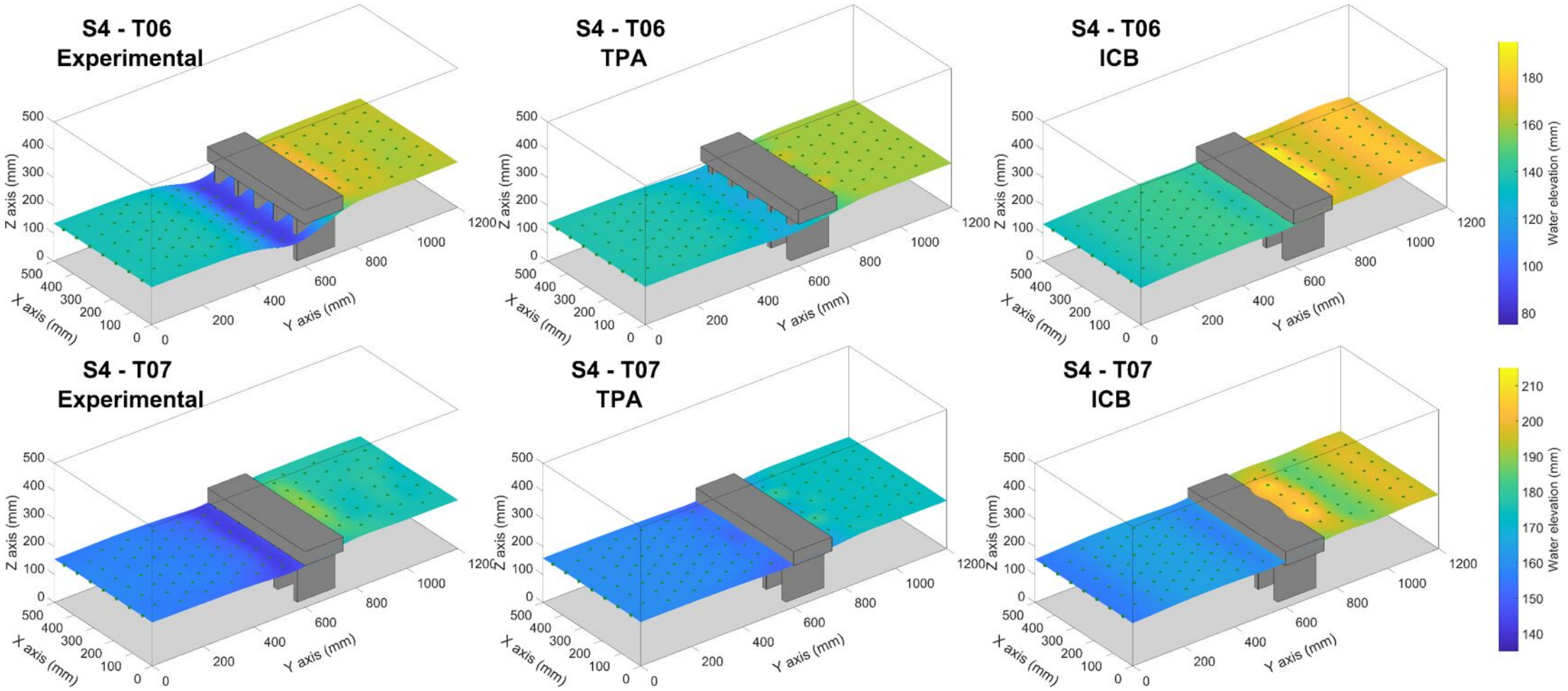

Fig 12

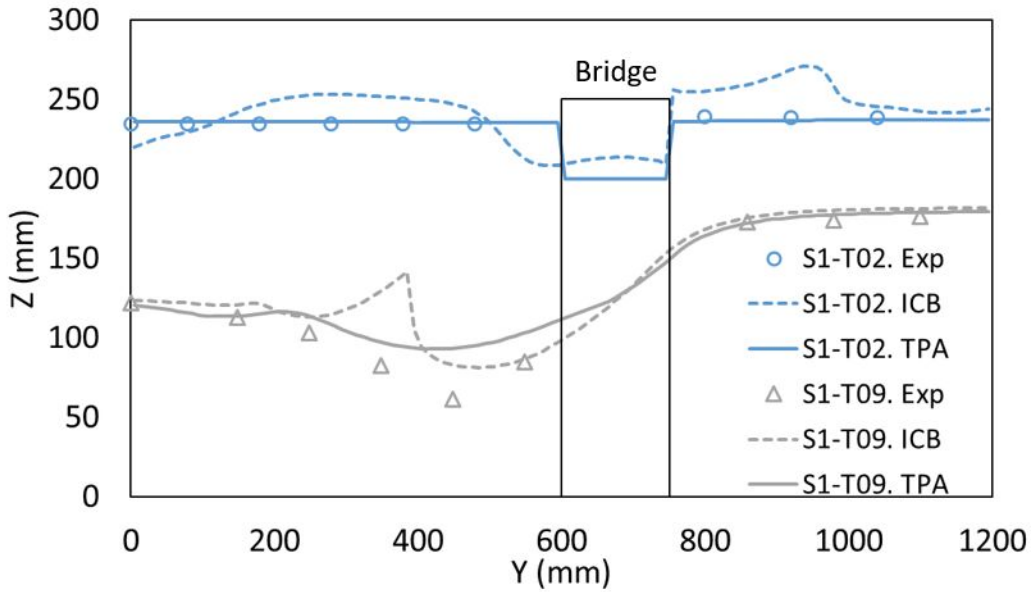

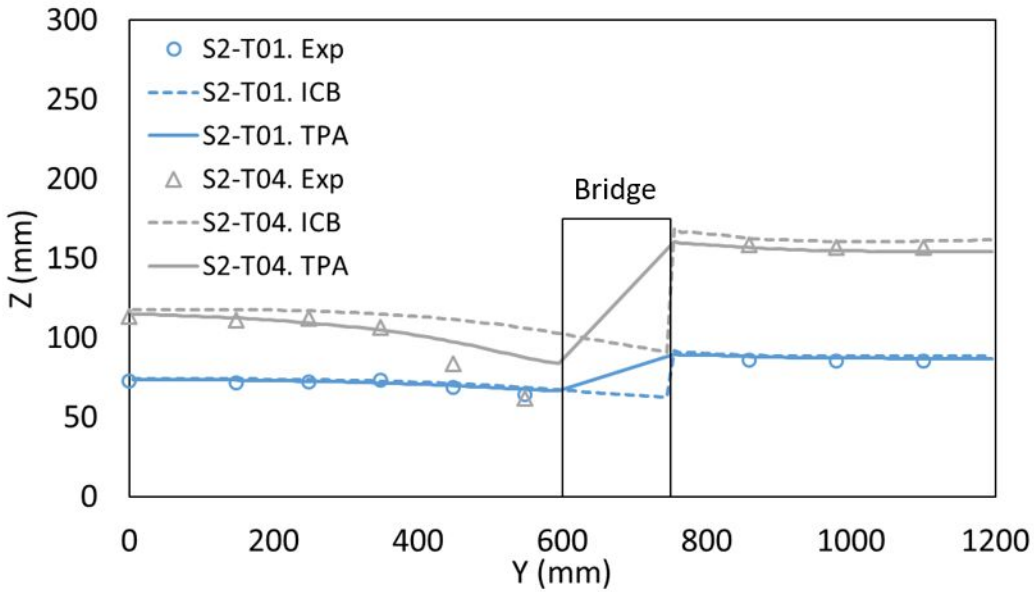

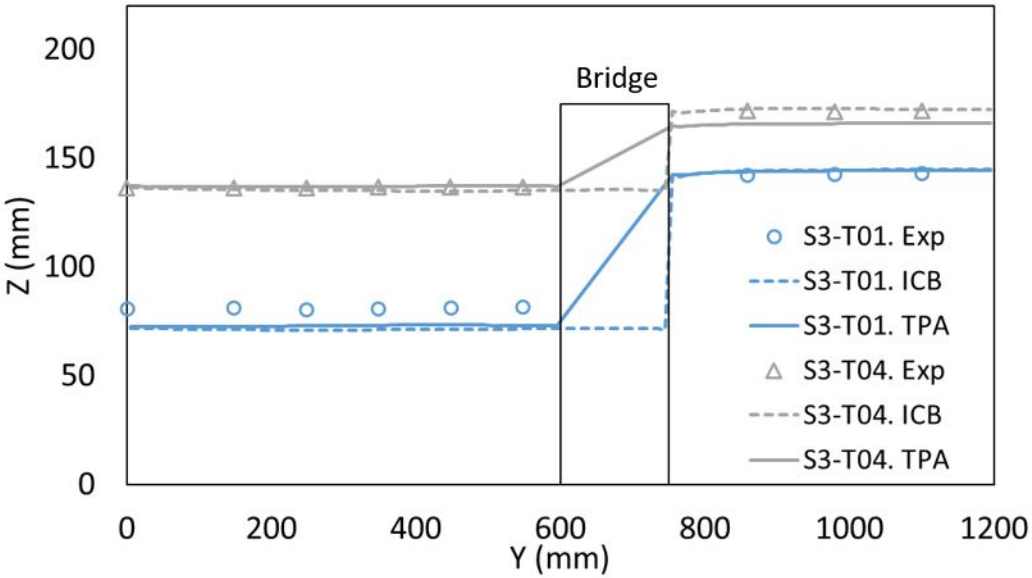

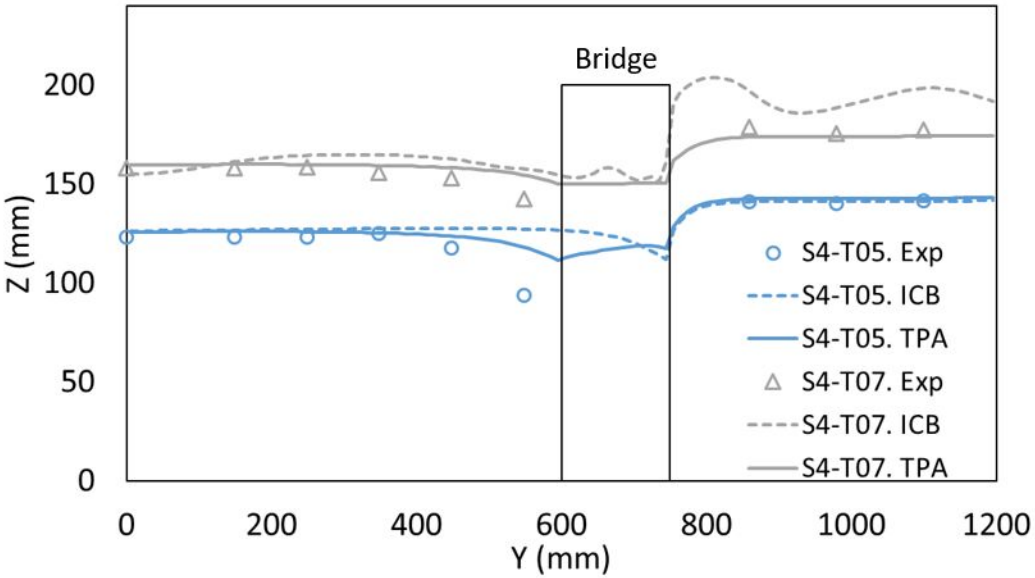

Fig 13